Journal of Chromatography A, 1218 (2011) 8432–8442

Contents lists available at SciVerse ScienceDirect

Journal of Chromatography A

journal homepage: www.elsevier.com/locate/chroma

Extending reversed-flow chromatographic methods for the measurement of diffusion coefficients to higher temperatures

W. Sean McGivern*, Jeffrey A. Manion

National Institute of Standards and Technology, Chemical and Biochemical Reference Data Division, Gaithersburg, MD 20899-8320, USA

ARTICLE INFO

Article history:
Received 14 June 2011
Received in revised form 9 September 2011
Accepted 13 September 2011
Available online 19 September 2011

Keywords:
Diffusion coefficients
High temperature
Uncertainties

ABSTRACT

A reversed-flow gas-chromatography (RF-GC) apparatus for the measurement of binary diffusion coefficients is described and utilized to measure the binary diffusion coefficients for several systems at temperatures from (300 to 723) K. Hydrocarbons are detected using flame ionization detection, and inert species can be detected by thermal conductivity. The present apparatus has been utilized to measure diffusion coefficients at substantially higher temperatures than previous RF-GC work. Characterization of the new apparatus was accomplished by comparing measured binary diffusion coefficients of dilute argon in helium to established reference values. Further diffusion coefficient measurements for dilute helium in argon and dilute nitrogen in helium (using thermal conductivity detection) and dilute methane in helium (using flame ionization detection) were performed and found to be in excellent agreement with literature values. The measurement of these well-established diffusion coefficients has shown that specific experimental conditions are required for accurate diffusion measurements using this technique, particularly at higher temperatures. Numerical simulations of the diffusion experiments are presented to demonstrate that artifacts of the analysis procedure must be specifically identified to ensure accuracy, particularly at higher temperatures.

Published by Elsevier B.V.

1. Introduction

Combustion phenomena are increasingly modeled with detailed numerical simulations that depend on accurate representations of both chemistry and transport properties. For the past several decades the uncertainties in the rate constants of reactions found in chemical combustion mechanisms have been significantly greater than those of the transport properties. However, improvements in key rate constants coupled with improvements in transport models have caused a renewed interest in the uncertainties of transport properties, particularly high-temperature diffusion coefficients [1–3].

There have been few measurements of the diffusion coefficients of hydrocarbons at high temperatures over the last three decades, particularly for hydrocarbon species with more than two carbons [4]. The extrapolation of low-temperature data to combustion conditions, possibly exceeding 1500 K, is highly uncertain, and diffusion coefficient measurements at higher temperatures are needed to improve these simulations.

The intent of the present work is to construct and demonstrate a reversed-flow gas chromatography (RF-GC) apparatus to systematically examine the diffusion coefficients of combustion-relevant species over a wide temperature range (300 to 723) K. Here we report results in which there are comparison data from the literature that can be used to validate the present measurements. As discussed below, the analytical procedure developed previously as part of a series of RF-GC diffusion coefficient studies [5–16] has significant limitations on allowable flow rates and diffusion times, which are not typically important at low temperatures but become relevant at higher temperatures. Although the RF-GC methodology has been utilized for catalytic studies at similarly high temperatures [17–19], the present work explores the measurement of binary diffusion coefficients. Since RF-GC had been used for lower-temperature diffusion coefficients and higher-temperature catalytic studies with apparently good results, it was a logical choice to extend to higher temperatures, subject to a number of specific considerations described presently. In addition, our design allows for automation of data collection, making it an efficient choice for examining the large numbers of compounds of ultimate interest. Numerical simulations have been found to reproduce measured chromatograms

* Corresponding author. Tel.: +1 301 975 8705.
E-mail address: sean.mcgivern@nist.gov (W.S. McGivern).

0021-9673/$ – see front matter. Published by Elsevier B.V.
doi:10.1016/j.chroma.2011.09.035

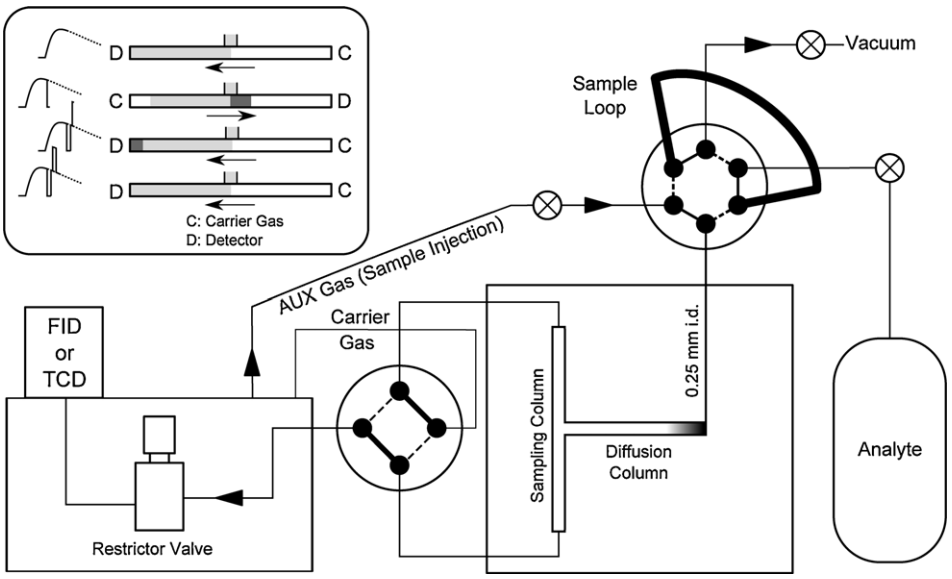

Fig. 1. Schematic diagram of apparatus for measuring binary diffusion coefficients with reversed-flow chromatography.

well and show a dependence on diffusion time and injection volume that was not explored in previous work with a similar apparatus.

2. Material and methods[1]

2.1. Apparatus

A schematic of the apparatus, based on the apparatus originally proposed by Katsanos and Karaiskakis [5], is shown in Fig. 1 and provides a means to monitor diffusion in a static environment (the "diffusion tube") continuously using gas chromatography. The major components are two separate "analytical" and "oven" Agilent 6890N gas chromatographs (GCs), a diffusion cell consisting of perpendicularly attached diffusion and sampling columns, two rotary valves (Vici Valco, Houston, TX) for flow reversal and sample injection, a sample bulb, and several on–off valves. The temperature of the diffusion column is controlled by the oven GC, which, with liquid nitrogen cryogenic cooling, can maintain temperatures in the range of (200 to 723) K, although presently we report measurements at 300 K and higher. Gas pressures, the switching and on–off valves, transfer line heating, and the flame ionization detector (FID) and thermal conductivity detector (TCD) are controlled by the analytical GC through the Agilent ChemStation software.

The diffusion and sampling columns are constructed from high-purity electropolished 316 stainless steel tubing (maximum surface roughness, R_a(max) = 0.25 μm) of outer diameter (OD) 6.35 mm (0.25 in.), and an inner diameter (ID) of 4.57 mm (0.18 in.). The columns are joined with an orbitally welded tee (Swagelok Microfit) with a diffusion tube length of (60.79 ± 0.01) cm. For the sampling column, equal lengths of 0.25 in tubing are welded to the tee, providing a total length of 81 cm for the larger diameter tubing. Each arm of the sampling column is then reduced to 3.18 mm (0.125 in.) OD electropolished tubing with a Microfit reducing union, which allows the tube diameter to decrease smoothly to reduce unswept volume. Zero dead volume fittings (Vico Valco) are then used to reduce the sampling column diameter to 1.59 mm (0.0625 in.) OD tubing. These tubes connect to a heated rotary valve as shown in Fig. 1. The output of the rotary valve for the sampling column passes through a micrometering needle valve (Vici Valco) contained within the oven GC and held at a fixed temperature, typically 313.2 K or 513.2 K. The temperature variation was used to ensure that the oven temperature had no effect on the measured diffusion coefficients. No variation was observed in the present studies, although additional consideration may be necessary for less volatile analytes. The needle valve may be switched between low-flow and standard fine-control versions, depending on the desired pressure for the experiment. Typically, the valve is set to provide a ~40 mL/min flow rate through the sampling column at the experimental pressure, which is sufficient to avoid artificially low diffusion coefficient determinations (vide infra). Due to the perpendicular geometry of the diffusion cell, the gas inside the diffusion tube is static.

Samples are injected at the head of the diffusion column using an automatic valve and loop system. A custom compression fitting (Vici Valco) attaches to the head of the diffusion column and is designed to direct the injection at a right angle relative to the column length precisely at the head of the column through a 0.5 mm orifice into a region with a bore size matching that of the diffusion column. Injection is accomplished by setting the auxiliary (AUX) gas pressure (Fig. 1) to be slightly greater, typically 13.8 kPa (2.0 psi), than that of the sampling column. The use of small ID tubing (0.25 mm ID) between the injection valve and column assures that no significant volume (<3% of the injection) of sample remains in the injection transfer tubing. The injection pressure and time are a function of the temperature of the experiment and are typically adjusted to give a ~0.2 mL injection (20% of the 1.0 mL sample loop volume) of sample over 6 s. True injection volumes are measured by comparing the integrated signal from standard timed injection with that from the injection of the entire sample loop. Integrated signals are determined by allowing the AUX gas to push the sample through the length of the diffusion tube to the detector after the injection. This analysis is performed in a separate run prior to each diffusion experiment.

The system pressure is a function of the temperature, carrier gas, and restrictor valve setting. The Agilent 6890 gas chromatograph monitors and actively maintains the pressure near the carrier

[1] Certain commercial materials and equipment are identified in this paper in order to specify adequately the experimental procedure. In no case does such identification imply recommendation of or endorsement by the National Institute of Standards and Technology, nor does it imply that the material or equipment is necessarily the best available for the purpose.

gas inlet and is capable of varying the pressure between (1.5 and 7.5) bar. The pressure in the static diffusion tube is slightly lower than the inlet pressure due to the pressure drop from the flow in the sampling column. Prior to each experiment, during the same run as the injection volume determination, the pressure at the head of the diffusion tube was obtained by setting the auxiliary pressure to zero and recording the actual pressure of the system with the analytical GC. This measurement was calibrated with a Mensor Model 2320 pressure gauge (accuracy 1.5×10^{-5} bar). The pressure drop over the length of the 4.6 mm I.D. diffusion tube itself is negligible, since the flow in the system is limited to the sampling column. Because the Agilent 6890 GC maintains the inlet pressures relative to ambient, changes in the absolute pressure in the diffusion tube are a function of atmospheric pressure. Since the tube pressure cannot be monitored during the diffusion experiment, the atmospheric pressure is continuously monitored using a calibrated Mensor Model 2320 manometer. Near the experimental pressures of ~400 kPa, we estimate the overall standard uncertainty in our reported absolute pressures to be 0.07%. Tube temperatures were measured using platinum wirewound resistance temperature detectors (Sensing Devices, Inc., Lancaster, PA) coupled to an Automatic Systems Laboratory Model F200 thermometer. The temperature detectors were calibrated with five points over the (300 to 723) K temperature range of the present study and have uncertainties ranging from (0.005 to 0.030) K in that range.

Reversal of the flow is accomplished via a pneumatically actuated 4-port rotary valve (Vici Valco) and allows gas in the sampling column to pass the diffusion column outlet multiple times. A second reversal to the original direction yields a negative–positive pair of peaks relative to the diffusion column output envelope. The nature of these peaks and the analysis of them to obtain the diffusion coefficient are discussed below. The Agilent ChemStation software does not allow a sufficient number of run-time events (valve reversals in the present experiment) necessary for these experiments. Custom software independent of the GC software was therefore written to overwrite the ChemStation run-time events after the reversals had taken place. This software allowed unattended operation of the system during the runs, which require at least 30 min each. The flow reversal events could be set at increments of 0.6 s and their timing and duration precisely and automatically controlled.

2.2. Samples

Methane was a high purity sample from Phillips Petroleum and was found to be greater than 99.9% pure by GC analysis. Nitrogen, and argon bath gas purities were stated to be 99.996% and 99.995%, respectively. The helium used as a bath gas was stated to be 99% pure. All carrier gases were passed through a thermal gas purifier (Restek, Bellefonte, PA) prior to use. We conservatively estimate that the purified helium was >99.9% pure from GC–mass spectrometry analysis with the primary contaminant being N_2, which is not affected by the purifier. Any errors in the measured diffusion coefficients as a result of impurities are expected to be well below the reported diffusion coefficient uncertainties.

Analyte samples were, for helium, argon, and nitrogen, neat gases. Methane was diluted in high-purity helium, at a concentration of 6.5% by volume.

2.3. Typical experimental conditions and assumptions

The rate of diffusion depends on temperature, pressure, and, to a lesser extent, concentration of the two diffusing components. Typical temperature dependences [20] are proportional to $T^{1.75}$ (temperature, T, in K) although the actual temperature exponent varies depending on the solute and bath gas. We have performed all experiments at temperatures ranging from 300 K to 723 K.

We report binary diffusion coefficients that have been scaled to 1.013 bar (1 atm) in inverse proportion to pressure, for consistency with typical diffusion coefficient reports [21]. Unscaled values and pressures are provided in the supplemental material. Previous experimental studies of the pressure dependences of the diffusion coefficients of all species in this study have been performed at (300 to 323) K [22–24]. For the species and pressures in the present work, the maximum deviation due to scaling is <0.15%. However, the pressure-dependent studies were done at mole fractions of the heavy component of 0.10–0.15; the validity of this scaling is unknown at the lower concentrations in this work. The temperature dependence of the pressure scaling is also unknown [23]. Further analysis of the pressure dependence falls outside the scope of the present work.

The use of reversed-chromatography for the measurement of the diffusion coefficient results in binary coefficients occurring at mole fractions for the bath gas that approach unity (dilute analyte). Simulations (vide infra) show that the maximum sample mole fraction at a point halfway down the diffusion tube is typically 0.02 when an undiluted solute is injected at the head of the diffusion column. Undiluted samples are used for experiments with the TCD detector, which has a lower sensitivity than the FID that is used for the CH_4 studies. Hydrocarbons in general will be diluted to ~5% or less, with the vapor pressure of the analyte at the temperature of the storage bulb being the primary constraint for larger species. Presently, we find no dependence of the measured diffusion coefficients on the initial sample concentration, although the injection volume and thus the linear extent of the tube initially charged with sample, must be kept small. In general, injection volumes in the present experiments are held to <3% of the total diffusion tube volume.

2.4. Analytical procedure

The conversion of reversed-flow chromatographic data, like that shown in Fig. 2, to a diffusion coefficient has been the subject of numerous previous publications [5,7,8]. Presently, we provide only a summary of the derivation of the governing diffusion equation in the system. Laplace transformation and algebraic rearrangement of Fick's second law in one dimension,

$$\frac{\partial c_z}{\partial t_0} = D\frac{\partial^2 c_z}{\partial z^2},$$

where z represents the diffusion tube coordinate, c_z is the concentration at z, t_0 is the time after sample injection, and D is the binary diffusion coefficient, yields a soluble algebraic expression if several simplifying assumptions are satisfied. In this case,

$$s \propto \exp\frac{-L^2/4D\tau}{\tau^{3/2}}, \quad (1)$$

where s is the reversal peak height, L is the diffusion tube length, and τ is the effective diffusion time. The effective diffusion time is given by

$$\tau = t_0 - t_M - \frac{1}{2}t_{FR}, \quad (2)$$

where t_M is the time required for a sample to flow from the output of the diffusion tube through one arm of the sampling column to the detector (the holdup time) and t_{FR} is the duration of the flow reversal. In practice, the measured chromatographic retention time, t_M, is corrected by t_0 and $1/2\ t_{FR}$ and a plot of $\ln s\tau^{3/2}$ vs $1/\tau$ is constructed, the slope of which is $-L^2/4D$. This data linearization procedure will be referred to as the "Laplace Transform Derived" (LTD) analysis for the remainder of this paper. One complication in the LTD fitting procedure is the well-known bias toward small signals when fitting linearized exponentially varying data with uncertainties that

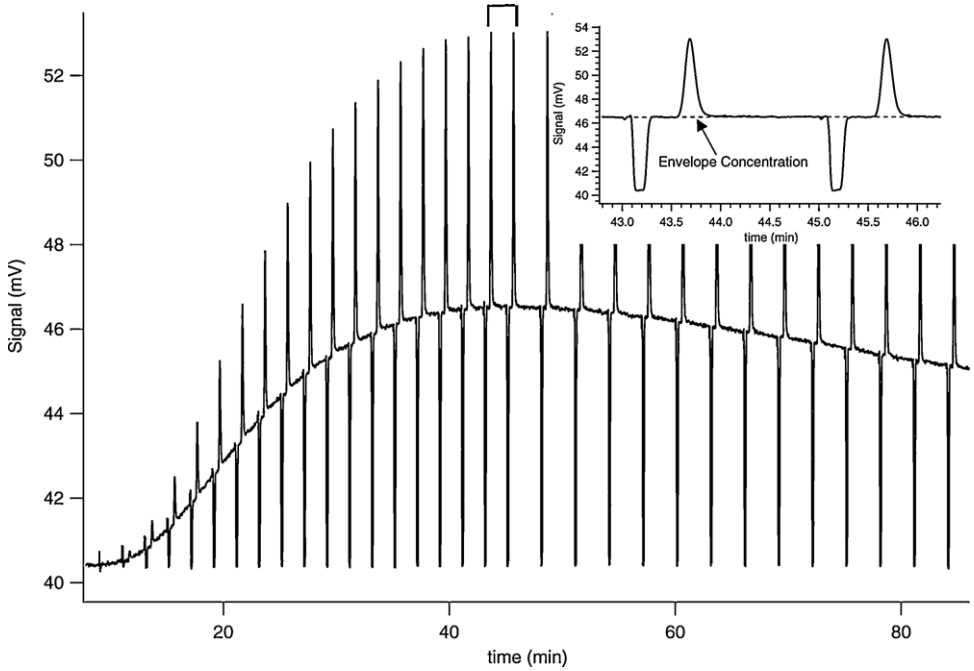

Fig. 2. Typical chromatogram used for determination of binary diffusion coefficients. These data show the diffusion of Ar in He at a temperature of 350.58 K and pressure 4.02 bar. The inset diagram shows a horizontal expansion of two reversal cycles.

do not represent a constant fraction of the data [25]. In the present system, the difference between a standard linear least-squares fit of the data and a correctly biased fit using estimated uncertainties from the analysis of the chromatogram was found to be negligible, and a linear fit of the $\ln s\tau^{3/2}$ vs $1/\tau$ plot was used throughout. All of the reported diffusion constants were obtained using this method. A typical plot and corresponding linear fit (dashed line) are shown in Fig. 3.

Several specific assumptions in the derivation must be satisfied for this linearity to hold true, and, as demonstrated by the long-time curvature in Fig. 3, the LTD-analyzed data is not linear at all times. The strong curvature at small $1/\tau$ values will be addressed in Section 4.2 below but is due to the breakdown of the assumptions used to derive Eq. (1). The first of these assumptions is the requirement that the flow rate in the sampling tube be sufficiently high that diffusion along the sampling tube axis is negligible. Additionally, the initial distribution of sample (the injected sample at the head of the diffusion tube) is assumed to be a Dirac delta function. Furthermore, there is a complex relationship between the length of the diffusion, total diffusion time, and flow rate required for Eq. (1) to hold over the entire measurement. Previous studies utilizing this methodology [4,5,7–9,11,13,14] have variously called attention to these assumptions. However, the implications of the breakdown of these assumptions have not been previously discussed, nor have the experimental conditions under which the breakdowns occur. In the present study, numerical simulations have been used to explore the limits of the total diffusion time (defined by the tube length and flow velocity) for various values of D as well as the shape and size of the initial sample distribution. Unless otherwise noted, all of the experimental data presented here have been taken under conditions in which Eq. (1) is satisfied.

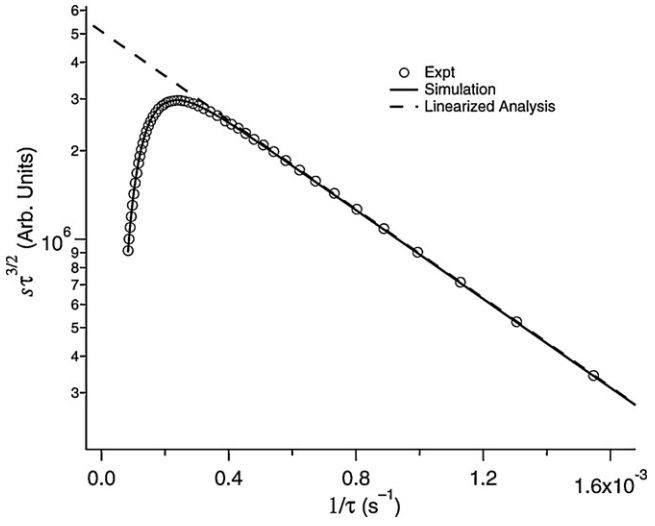

Fig. 3. Laplace transformation analysis for determination of diffusion coefficient of dilute CH_4 in He. Circles represent transformed experimental data ($s\tau^{3/2}$) and the dashed line is a linear fit. The solid line is the result of a numerical simulation (see text). Data pertain to 599.9 K and 4.032 bar $D(1.013\,\text{bar}) = 2.146\,\text{cm}^2\,\text{s}^{-1}$.

3. Results

3.1. Reversal chromatograms

Fig. 2 shows a typical chromatogram from the thermal conductivity detector; chromatograms from the FID have similar features. A broad envelope of signal is due to analyte exiting the diffusion tube after diffusing from the point of injection (inset of Fig. 2). The upward and downward peaks superimposed on that envelope are due to the flow reversal cycles discussed in the previous section. The inset diagram shows an expansion of two reversal cycles. Reversal of the flow through the sampling column (inset Fig. 1) with the four-port rotary valve induces pure bath gas to reach the detector, causing the signal to drop to its baseline value, as shown by the downward-facing peaks in the figure. After 4.2 s (0.07 min), the valve is rotated again, allowing the system to continue flowing through the sampling column in the original direction. During this reversal period, sample exiting the diffusion tube diffuses into gas in the sampling column that already has the envelope concentration of analyte (dashed line, Fig. 2 inset). This added analyte results

Table 1
Binary diffusion coefficients for Ar and He. Entries on the left side of the table ("Ar–He") are dilute Ar in He results, and entries on the right ("He–Ar") are dilute He in Ar. All diffusion coefficients have been scaled to 101.3 kPa (1 atm). σ is one standard deviation, and n is the number of repeated measurements at a given temperature.

	Ar–He				He–Ar			
Nominal T (K)	n	D (cm^2 s^{-1})	2σ	$2\sigma/D$ (%)	n	D (cm^2 s^{-1})	2σ	$2\sigma/D$ (%)
300	15	0.734	0.0044	0.59	14	0.749	0.0059	0.79
350	15	0.954	0.0035	0.37	4	0.973	0.0099	1.0
400	9	1.192	0.008	0.65	7	1.206	0.009	0.71
450	4	1.447	0.012	0.85	4	1.475	0.010	0.67
500	6	1.719	0.015	0.86	7	1.758	0.016	0.80
550	6	2.017	0.022	1.1	4	2.068	0.022	1.1
600	6	2.329	0.035	1.5	4	2.382	0.040	1.7
650	5	2.676	0.049	1.9	3	2.724	0.058	2.1
700	5	3.023	0.084	2.8	3	3.103	0.088	2.8
723	5	3.193	0.095	3.0	3	3.306	0.108	3.3

in a peak in the concentration chromatogram that then returns to the envelope value in approximately the same time as the reversal.

The height of this peak above the baseline is linearly related to the concentration of analyte exiting the diffusion tube at the effective reversal time (Eq. (2)). However, to correct for the inevitable instrumental drift over the long timescales (thousands of seconds) of a typical diffusion experiment, the peak height is measured relative to the envelope value. Concentrations for each peak are derived by fitting a line through the envelope on each side of the reversal cycle and taking the difference between the fitted line and the peak height. The peak height is determined by taking the maximum value of a parabola fitted to a 5 s window surrounding the maximum peak signal value of the peak, ten points on the 0.5 Hz sampling rate used in the present experiments [26].

3.2. Diffusion coefficients

As part of a systematic examination of the methodology, we have utilized our apparatus to determine the binary diffusion coefficients of four reference systems (dilute analyte–bath gas): Ar–He, He–Ar, N_2–He, and CH_4–He. The first two of these systems have very well-established diffusion coefficients and have been previously employed [27] for system calibration. Additionally, a comparison of the measurements for mixtures dilute argon in helium and dilute helium in argon measurements provides a test of our ability to accurately determine small variations in D. The nitrogen–helium system likewise has well-established experimental values and is used for further validation of the present methodology. The data for systems of Ar, He, and N_2 were taken using a thermal conductivity detector (TCD). Flame-ionization detectors (FID) are much more sensitive for the organic compounds of primary interest to combustion scientists and will be the primary detector utilized in future work. The CH_4–He system, although not as well characterized as the diffusion of nonreactive gases, provides validation data for this configuration. Binary diffusion coefficients for Ar–He, He–Ar, He–N_2, and CH_4–He are given in Tables 1–3, respectively, for temperatures from (300 to 723) K. Reported uncertainties are two standard deviations and include systematic effects from temperature and other sources of error, as discussed in the following section. In each case, the diffusion coefficients have been scaled linearly to 101.3 kPa (1 atm) pressure. The primary (unscaled) data are provided in the supplementary material.

These data are plotted in Figs. 4–7 as open circles with error bars showing uncertainties to two standard deviations. In each figure, the lower plot is the diffusion coefficient in cm^2 s^{-1} and the upper plot is the deviation of the diffusion coefficients from fits to the temperature dependences of D as follows. Each point in a deviation plot represents the average of multiple runs at slightly different temperatures. The runs were individually corrected to a single "nominal" temperature shown in Tables 1–3 using a temperature dependence derived from all measured points of the form $a(T/1\,\mathrm{K})^n$, where T is the temperature in K, and a and n are parameters. These parameters are reported in Table 4. This correction to the diffusion coefficient for any individual point is less than 0.85% across the entire range of temperatures and is derived from temperatures differences of less than ±1.5 K between the reported and actual temperatures. In the figures, the fitted temperature dependences are shown as solid lines. For simplicity, the uncertainties in the parameters in Table 4 were derived from the temperature-corrected data shown in Tables 1–3 at the nominal temperatures rather than the full data set.

Table 2
Binary diffusion coefficients for dilute N_2 in He. All diffusion coefficients have been scaled to 101.3 kPa (1 atm). σ is one standard deviation, and n is the number of repeated measurements at a given temperature.

Nominal T (K)	n	D (cm^2 s^{-1})	2σ	$2\sigma/D$ (%)
300	8	0.710	0.0046	0.64
350	6	0.914	0.0041	0.45
400	5	1.143	0.007	0.65
450	2	1.381	0.011	0.83
500	5	1.658	0.017	1.0
550	3	1.934	0.022	1.1
600	3	2.237	0.034	1.5
650	2	2.564	0.047	1.8
700	2	2.903	0.082	2.8
723	2	3.071	0.090	2.9

Individual diffusion coefficient data from the previous literature are given by the indicated symbols with literature temperature dependences indicated by dashed lines. All of the systems considered here have been the subject of previous reviews, and much of the older data have been superseded by newer more accurate determinations. We present only the reference data derived from critical evaluations together with selected data showing representative values obtained with various techniques of interest. The reader is

Table 3
Binary diffusion coefficients for dilute CH_4 in He. All diffusion coefficients have been scaled to 101.3 kPa (1 atm). σ is one standard deviation, and n is the number of repeated measurements at a given temperature.

Nominal T (K)	n	D (cm^2 s^{-1})	2σ	$2\sigma/D$ (%)
300	21	0.674	0.0042	0.62
350	10	0.874	0.0047	0.53
400	15	1.087	0.005	0.50
450	7	1.322	0.008	0.60
500	12	1.579	0.012	0.79
550	7	1.854	0.019	1.0
600	6	2.144	0.030	1.4
650	6	2.456	0.046	1.9
700	6	2.792	0.078	2.8
723	6	2.943	0.087	3.0

Table 4
Fitting parameters for temperature dependence of the binary diffusion coefficient of the form $D_{fit} = a(T/1\,K)^n$, where T is the temperature in K. Uncertainties (σ_x) in the parameters are one standard deviation derived from a nonlinear fit of the aggregate data in Tables 1–3.

Diffusion pair[a]	a ($cm^2\,s^{-1}$) × 10^5	σ_a ($cm^2\,s^{-1}$) × 10^5	n	σ_n	D_{fit}($cm^2\,s^{-1}$) [300 K]
Ar–He	5.56	0.19	1.664	.006	0.736
He–Ar	5.34	0.24	1.674	.007	0.749
N_2–He	5.54	0.21	1.658	.006	0.709
CH_4–He	4.97	0.18	1.668	.006	0.673

[a] The first listed component is the dilute analyte, and the second component is the bath gas.

referred to the previous critical evaluations identified in the figures for a more complete assessment of the extant data.

Marrero and Mason have provided recommendations for all of the systems in this work based on a critical review of direct diffusion measurements and derivations from molecular beam data [28]. The estimated uncertainty (1σ) of those recommendations including Ar, He, and N_2 varies with temperature from 1% at 300 K to ~3% at 723 K with a larger uncertainty range for the CH_4–He system as discussed below. In the figures, the Marrero–Mason recommended diffusion coefficients are indicated by dot-dash lines; the uncertainties were not included in the figures for clarity. The temperature exponents recommended by Marrero and Mason are larger than observed in this work, substantially impacting the agreement at higher temperatures.

3.2.1. Argon–helium

Argon in helium has an extremely well-established diffusion coefficient that shows a small but measureable concentration dependence, approximately a 3% increase as the mole fraction of Ar increases from zero to one in the diffusion mixture [27]. The presently determined diffusion coefficients, given in Table 1, show diffusion coefficients for dilute He in Ar and dilute Ar in He separately. Figs. 4 and 5 show a comparison between the present measurements and literature data. The dashed line and surrounded shaded field are calculations from Kestin and coworkers [29] of the diffusion coefficients based on a global best-fit of Chapman–Enskog calculated diffusion coefficients to a critically evaluated dataset for various combinations of He, Ne, Ar, and Kr. The He–Ar fit was

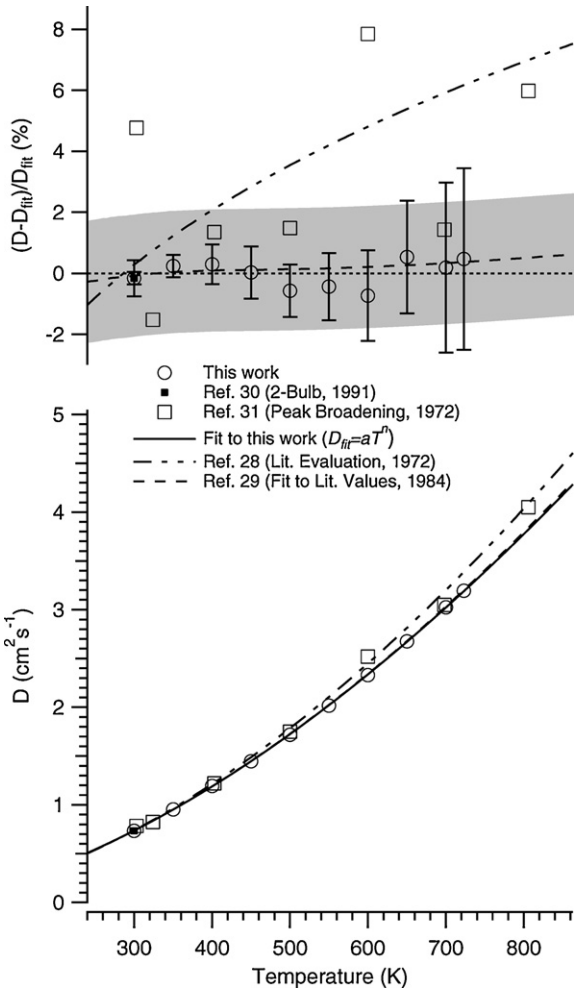

Fig. 4. Binary diffusion constants for dilute Ar (<100 ppm V/V) in He between 300 K and 723 K. The lower graph shows the diffusion coefficients (uncertainties not shown for clarity – see Table 1), and the upper chart shows the deviation from the temperature-dependent fit to the present data. Data sources and measurement techniques are indicated in the inset.

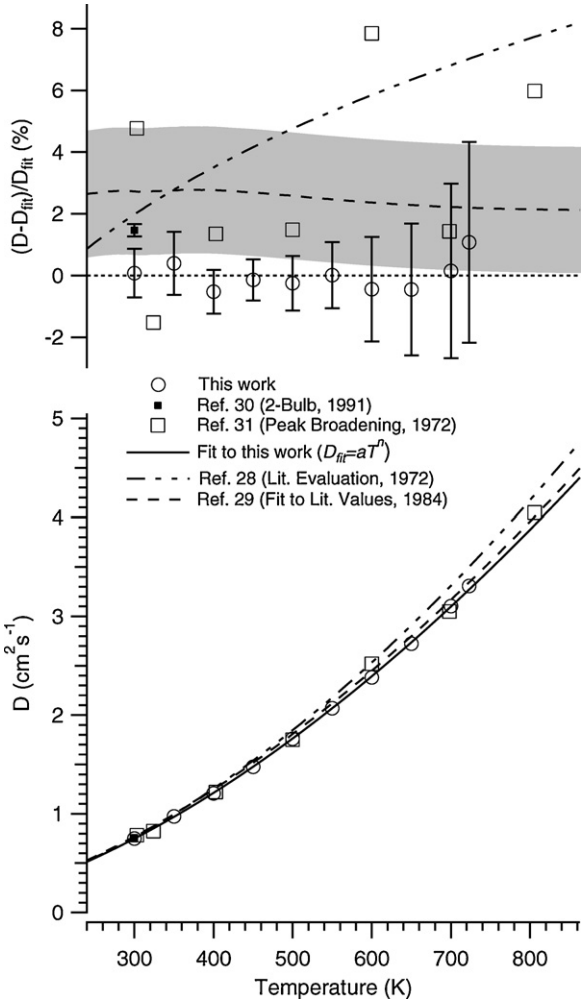

Fig. 5. Binary diffusion constants for dilute He(<100 ppm V/V) in Ar between 300 K and 723 K. The lower graph shows the diffusion coefficients (uncertainties not shown for clarity – see Table 1), and the upper chart shows the deviation from the temperature-dependent fit to the present data. Data sources and measurement techniques are indicated in the inset.

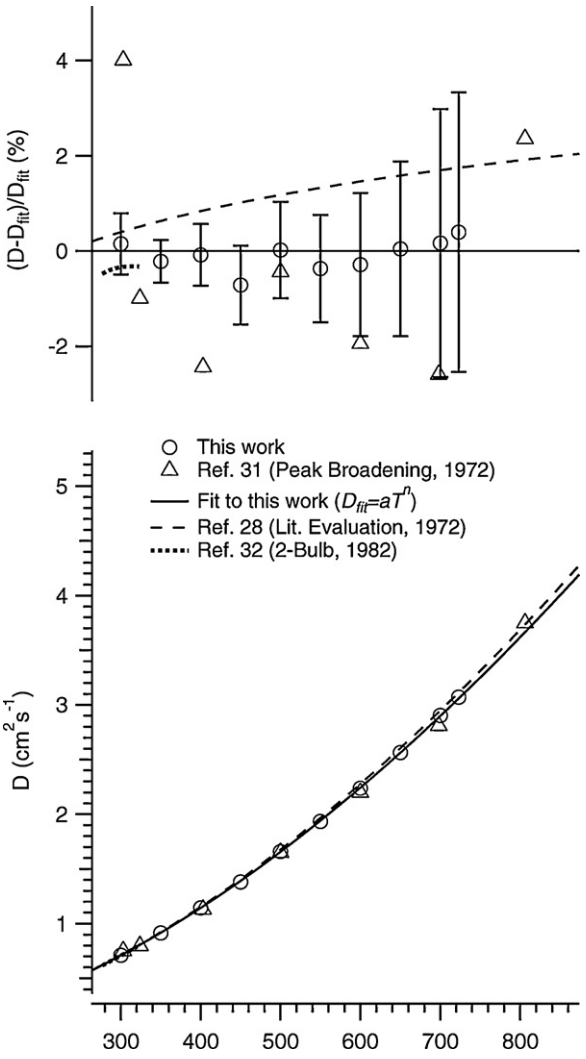

Fig. 6. Binary diffusion constants for dilute N_2(<100 ppm V/V) in He between 300 K and 723 K. The lower graph shows the diffusion coefficients (uncertainties not shown for clarity – see Table 1), and the upper chart shows the deviation from the temperature-dependent fit to the present data. Data sources and measurement techniques are indicated in the inset.

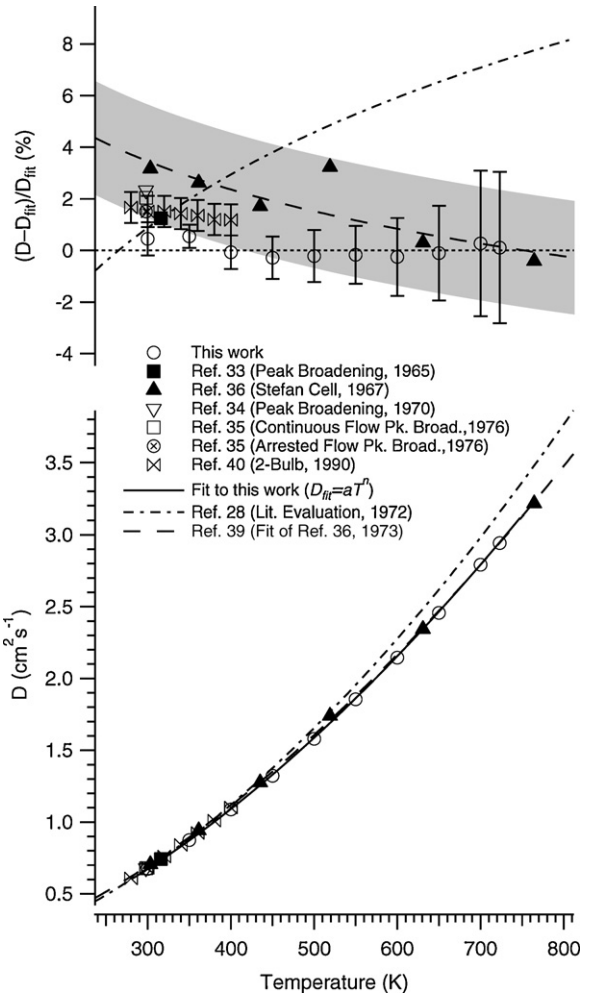

Fig. 7. Binary diffusion constants for dilute CH_4(<100 ppm V/V) in He between 300 K and 723 K. The lower graph shows the diffusion coefficients (uncertainties not shown for clarity – see Table 1), and the upper chart shows the deviation from the temperature-dependent fit to the present data. Data sources and measurement techniques are indicated in the inset.

estimated to have an uncertainty (assumed by us to be 1σ) of 1%. The data point at 300 K, shown as a filled square in Fig. 4 (Ar–He), is the infinite reference dilution value from the critical review of Wakeham et al. [30] This data point was used as a means to correct small systematic errors in the present system from the diffusion tube length measurement as discussed in detail below. In this case, the agreement between the present data and that point is forced.

For comparison, we also show the results obtained by Liner and Weissman [31] using the GC peak broadening technique (unfilled squares in Figs. 4 and 5). These show moderately good agreement although the scatter in the data appears significantly larger with that methodology. Liner and Weissman estimated their uncertainty at 3–5%. Additionally in both systems, the recommended temperature dependence of Marrero and Mason shows good agreement at 300 K but overestimates the present work at higher temperatures. The present data, however, does agree with the Marrero and Mason temperature dependence to within their respective 2σ uncertainties.

Fig. 8 shows the differences between the measured diffusion coefficients for He–Ar (unity mole fraction Ar) and Ar–He (unity mole fraction He) as a fraction of the Ar–He values. The 300 K Ar–He diffusion coefficient was used to determine the effective length of the diffusion tube in the present work and was therefore fixed. At all temperatures, the diffusion coefficients were found to be higher for the dilute argon in helium, in qualitative agreement with literature values. However, the solid line in the figure is a literature reference value, and the present results are distinctly lower. At

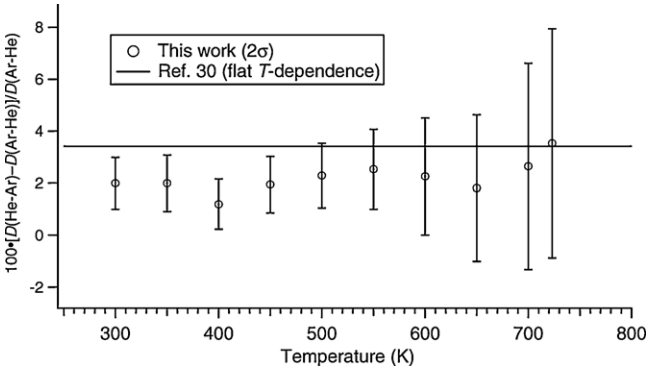

Fig. 8. Fractional difference between diffusion coefficients for dilute helium in argon relative to dilute argon in helium. Circles represent our experimental data; the solid line is derived from the data of Ref. [30] at 300 K with an assumed flat temperature dependence based on the Chapman–Enskog predictions of Ref. [29].

300 K, the reference value shown in the figure was determined from the recommendations of Wakeham et al. [30] based on the two-bulb measurement of Ref. [27]. The temperature dependence was assumed to be flat, which is consistent with Chapman–Enskog (CE) calculations using the interaction potentials suggested by Kestin and coworkers for the Ar/He system [29]. However, it should be noted that the CE-calculated 300 K diffusion coefficients of Kestin and coworkers vary from the Wakeham et al. recommendations, lying 1.1% higher than the 3.4% variation recommended by Wakeham.

3.2.2. Nitrogen–helium

Data for the binary diffusion coefficient of dilute nitrogen in helium is shown in Fig. 6 with corresponding numerical data in Table 2. In general, fewer repeated runs were used in these measurements than in the other systems considered presently, and these represent a more reasonable data set size. Establishing the uncertainty of fewer runs will become especially important with larger compounds with substantially lower diffusion coefficients and correspondingly longer measurement times. The present work shows good agreement with the calibrated two-bulb measurements of Trengove and Dunlop [32], which were taken at temperatures near 300 K. Also shown are the GC peak-broadening results from Liner and Weissman [31], which have an estimated uncertainty of (3–5%) and also show good agreement with the present data. Finally, the Marrero and Mason [28] recommendations reproduce the low-temperature data well but show an increasing deviation with temperature. However, the agreement between these recommendations and the present data for nitrogen–helium is better than observed in the other systems discussed.

3.2.3. Methane–helium

Results for dilute methane in helium are presented in Fig. 7. The concentration of the diffusing methane was measured using the flame ionization detector rather than with thermal conductivity as in the other systems. This arrangement is typically how hydrocarbon diffusion coefficients will be studied, and the methane–helium system provides a sound validation data set. As may be observed from the deviation plot, the present data reproduce the previous measurements well, although the present results are generally lower than the previous determinations. Numerous measurements have been made near room temperature, and the present work agrees well with most of this previous work [24,33–36]. Several recommendations have also been made for higher temperatures. The recommended temperature dependence of Marrero and Mason [28] is shown. However, those authors chose to fix the temperature exponent to yield $D \propto T^{1.75}$ based on the work of Fuller et al. [37,38]. In this work, we observe a temperature exponent of 1.668 ± 0.006, and the present data lie well below the Marrero and Mason recommendations. Nonetheless, the estimated uncertainty of the Marrero and Mason recommendation ranges from (3 to 7)% from (300 to 723) K, and the present data are consistent within those uncertainties.

Frost utilized a Stefan cell to measure the CH_4–He diffusion coefficients and reported experimental data [36] and a fit [39]. In these experiments the average mole fraction of methane in the cell gas mixtures was 0.13 to 0.31, much larger than our highly diluted analytes. The present results are nonetheless in reasonable agreement with those measurements, especially at higher temperatures. The present results also show good agreement with more recent experimental work by Dunlop and Bignell, carried out with a two-bulb apparatus over a narrower temperature range [40]. These same authors later calculated [24] the temperature-dependence of the CH_4–He diffusion coefficient based on thermal diffusion factors and viscosities, deriving a slightly higher temperature exponent than observed in the present work (Table 4). Not shown in Fig. 7 is the 1982 result of Katsanos and Karaiskakis, who utilized the same reversed-flow GC technique as in the present work but obtained a value of the diffusion coefficient [$D(296.7\,\mathrm{K}) = 0.522\,\mathrm{cm^2\,s^{-1}}$ at 1 bar] that is approximately 20% lower than the other determinations, including this work [5]. The reason for this discrepancy is not clear.

4. Discussion

4.1. Uncertainty analysis and minor corrections

Uncertainty estimates provided throughout this study are two standard devations unless otherwise noted.

4.1.1. Length

As shown in Eq. (1), the diffusion coefficient depends on the square of the diffusion tube length, and uncertainty in the tube length is thus a significant source of uncertainty in D [4]. Length measurements were made with a 1.1 m caliper (Mitzuno) and a precision measuring tape (Starrett), providing an uncertainty in the length of the straight tube of 0.1 mm for the 60.79 cm tube (prior to bending to fit into the oven) used in this study. The lengths of the diffusion columns are corrected at each temperature above room temperature for the thermal expansion of the stainless steel with a thermal expansion coefficient [21] of $1.73 \times 10^{-5}\,\mathrm{K^{-1}}$.

However, additional length uncertainties are present due to the intersection of the diffusion and sampling tubes and the necessary bending of the diffusion tube to fit into the GC oven. The intersection of the two cylindrical tubes yields a total tube length that varies by half of the inner tube diameter (half of 4.6 mm) over the radial dimension of the diffusion tube. The apparent length used for the determination of the diffusion coefficient using the one-dimensional treatment in Eq. (1) will lie between these extremes and depends on the spatial distribution of the sample exiting the diffusion tube. In addition, the diffusion tube was bent into a 5″ radius half circle in order to fit into the gas chromatograph oven. Assuming that the metal does not significantly compress along the inner diameter, the length will vary an additional 14.4 mm between the inner and outer walls of the diffusion tube.

We have elected to account for these uncertainties by obtaining an effective tube length, L_{eff}, from a comparison of the measured diffusion coefficients of dilute He in Ar with the literature. Specifically, we have chosen the 300 K data reported by Wakeham et al. for the infinite dilution of He in Ar [30], $(0.7344 \pm 0.0042)\,\mathrm{cm^2\,s^{-1}}$ at 1.013 bar (2σ uncertainty). This value is identical to the 1977 measurements of Dunlop and coworkers [27] obtained in a Loschmidt-type cell; however, the estimated uncertainty was decreased from 0.6% to 0.1% in the later review. We have taken the latter uncertainty value as 1σ in the present study. These results were subsequently used by Dunlop and Bignell to calibrate their two-bulb apparatus [40]. The present data were taken at temperatures of (300.47 ± 0.01) K and were corrected using the measured temperature dependence (Table 4) to 300.00 K. From this analysis, we find a value of L_{eff} of (61.28 ± 0.01) cm provides the best fit. This value of L_{eff} was used throughout the present study.

4.1.2. Temperature

Temperature measurements were made at short time intervals during experiments simultaneously at three points along the length of the diffusion tube. Calibrated platinum resistance temperature detectors were placed at the top of the diffusion tube (near the inlet), near the lowest point in the oven, and at the approximate midpoint between these extremes. Small thermal gradients are present at higher temperatures and were found to lie primarily along the vertical axis of the oven. The temperature along

the length of the diffusion tube varied by typically 0.03 K for the 300 K experiments (0.1%) up to 5.0 K for the 723 K experiments (0.69%). We have conservatively assumed that the uncertainty in the temperature is given by this maximum deviation (i.e. ±2.5 K for the 723 K experiments) and expect these estimates to provide reasonable upper limits to the individual temperature uncertainties. This temperature variation is the dominant source of uncertainty in the high-temperature experiments, since the diffusion coefficient in this temperature range typically varies as $\sim T^{1.7}$. This is the value assumed when calculating the effects of the temperature uncertainty on the measured diffusion coefficients.

4.1.3. Flow rates and Reynolds number

Flow rates through the sampling column must be kept reasonably high to ensure that the Laplace transform analytical procedure in Eq. (1) remains valid. Typically, the restrictor valve, which is held at a constant temperature in the analytical GC oven during diffusion experiments at all temperatures, is set to give flow rates of ~40 mL/min (all flow rates reported in the manuscript refer to volumetric flow at a temperature of 298 K and 1.013 bar pressure). To explore the effects of the flow rate, we performed experiments at constant pressure at 300 K and varying flow rates through adjustment of the valve contained with the analytical oven. At lower flow rates, the individual reversal peaks were significantly broadened through diffusion in the sampling column, which violates the assumptions in the derivation of Eq. (1). Measured diffusion coefficients were found to be substantially lower at lower flow rates, but increase as the flow rate is raised until an apparently asymptotic value is reached at a flow of ~35 mL/min.

The 40 mL/min flow rate used in the present work leads to flow tube velocities of 2.0 cm s^{-1} and 4.9 cm s^{-1} at 300 K and 723 K, respectively, at 2 bar pressure. Under the most extremely turbulent conditions of low temperature and gas viscosity (N_2), the Reynolds Number does not exceed 12, and the flow is fully laminar. No transport other than through diffusion is expected to occur between the sampling column and diffusion tube. We have thus made no corrections to the data to account for mixing due to flow at the crossing point of the diffusion and sampling columns.

A flow of 40 mL/min prevents the flame ionization detector (FID) from lighting, although a stable flame may be obtained with such a flow. In order to use the FID, the flow must first be decreased, the flame lit and stabilized, and the flow subsequently increased. This does not appear to introduce any noise or instability in the FID output and was used throughout the methane–helium measurements. Despite these difficulties, such a flow rate is crucial in obtaining accurate diffusion coefficients using the LTD method, irrespective of the other analytical considerations presented in this manuscript.

4.1.4. Nonlinearity of LTD analysis

The Laplace transform analysis performed by linear fits of semilog plots of data transformed according to Eq. (1) introduces uncertainty beyond the uncertainties discussed previously, particularly for higher temperatures. At long times, the plot of $\ln s\tau^{3/2}$ vs $1/\tau$ shows a distinct nonlinearity, ultimately coming to a maximum, as shown in Fig. 3. This nonlinearity is simply an artifact of the LTD analysis assumptions and has no physical meaning. The time at which the nonlinear portion of the plot significantly affects the linear fit (and thus the diffusion coefficient) decreases with increasing temperature. Since the number of reversal events in a given time is limited by the holdup time of the gas in the sampling column during the reversal, fewer points are thus available for a linear analysis as the temperature increases. At the highest temperatures, few points (typically six to eight) fall within the linear region, which increases the uncertainty of the nonlinear fits. This effect can be qualitatively observed from increasing standard deviations in D with increasing temperature (supplemental information), although quantitative determination is precluded by other random uncertainties. In the present work, the larger values of σ_D at the higher temperatures shown Tables 1–3 are due to the temperature uncertainty as discussed above. As demonstrated from the simulations described below, it would be possible, in principle, to obtain diffusion coefficients by fitting the results of a numerical simulation of the time-dependent concentrations in the diffusion tube to the entire data set including the nonlinear regime. However, this procedure is extremely computationally intensive and would require a detailed Monte Carlo analysis for estimating the uncertainty. Such an analysis is not justified, since the primary contributor to the uncertainty is from temperature.

In any case, the presence of this nonlinear region in the LTD analysis plots can have a significant influence on the measured diffusion coefficient at times well before the turnover time. By eye, fits to data including the linear and early nonlinear region appear to reproduce the data well. However, these "early turnover" points universally decrease the slope and lead to artificially high diffusion coefficients with errors far exceeding the computed uncertainties. An effective means to determine if these regions of nonlinearity are biasing fits is to fit the expected linear region with both a linear least squares fitting algorithm of the semilog plot and a nonlinear least squares algorithm, such as Levenberg–Marquardt [26], of the direct transform. Deviations of the parameters derived from these analysis, particularly in the temperature exponent, are indicative of interference resulting from the breakdown of the LTD analysis approximations. The diffusion coefficients in the present work were all calculated by both methods, and linear and nonlinear fits were mutually consistent.

4.2. Simulations

We have utilized numerical simulations to evaluate the effects of the various experimental parameters on the measured diffusion coefficients. Using these simulations, we have established limits on the applicability of Eq. (1) for determining the correct diffusion coefficient from the measured chromatograms. In these systems, only the concentrations within the diffusion tube were simulated; it was assumed that molecules that exit the diffusion tube are detected immediately (zero hold-up time) with a constant dilution factor due to the flow and no diffusion. Under our typical conditions, the diffusion in the sampling tube is small, as evidenced by the sharp reversal peaks with widths close to the reversal times (Fig. 2), and the flow rate was sufficiently high that the minor longitudinal diffusion in the chromatography tube had little impact. The heights of the reversal peaks are therefore expected to be proportional to the concentration of the sample exiting the diffusion column at the corrected reversal time, τ (Eq. (2)). Simulations of the output concentration were then analyzed as if they were data where the simulation time was considered equivalent to τ without regard for the reversals in the simulation.

Numerical simulations of the diffusion within the diffusion tube were performed using a standard Crank–Nicolson (CN) algorithm [41] implemented in the Python scripting language. In the CN algorithm, the diffusion tube concentration distribution at a specific time, $c(z, t)$ is discretized along a fixed spatial grid $z_i = z_0 + i\Delta z$, where the subscripts represent the spatial grid index. This distribution is allowed to evolve in time from an initial distribution, $c(z, 0)$, such that $t^n = t^0 + n\Delta t$ with the superscripts representing the time index. The change in the concentration distribution from t^n to t^{n+1} is given by

$$\frac{c_i^{n+1} - c_i^n}{\Delta t} = \frac{D}{2}\left[\frac{c_{i+1}^n - 2c_i^n + c_{i-1}^n + c_{i+1}^{n+1} - 2c_i^{n+1} + c_{i-1}^{n+1}}{(\Delta z)^2}\right],$$

where $c_i^n \equiv c(z_i, t^n)$. Solution of this implicit equation requires the inversion of a tridiagonal matrix at each time step. This

numerical inversion may be done efficiently [42], and the use of the CN algorithm allows a substantially larger timestep than in a fully explicit scheme. Typically, a 400-point spatial grid over the length of the diffusion tube was used, with timesteps ranging from 0.1 s to 0.5 s. Boundary conditions for the system were taken as

$$\left.\frac{\partial c(z,t)}{\partial z}\right|_{z=0} = 0 \text{ and } -D\left.\frac{\partial c(z,t)}{\partial z}\right|_{z=L} = vc(L,t),$$

where v is the flow velocity (cf. Eq. (5) of Ref. [5]). Due to the assumption that diffusion does not occur in the sampling column, the input flow rate affects only the boundary condition at $z = L$ within the simulation.

4.2.1. Long-time curvature

As noted in the previous section, we observed experimentally that the LTD analysis plot of $\ln s\tau^{3/2}$ vs $1/\tau$ was initially linear but became strongly curved at longer times, as is clearly demonstrated in the data shown in Fig. 3. The time at which this curvature began to significantly affect the determination of the absolute diffusion coefficient (D in Eq. (1)) was also found to decrease with increasing D. Simulations confirm this curvature as shown by the excellent agreement between the LTD-analyzed simulation (solid line) and LTD-analyzed data (open circles) in Fig. 3. In calculating the concentration profile used to generate the solid line in Fig. 3, the diffusion coefficient determined from the LTD-analyzed experimental data was used. The excellent agreement between the simulation and experiment demonstrates that the curvature is an artifact of the fitting procedure due to a breakdown in the assumptions of the LTD analysis at longer times rather than a physical effect.

4.2.2. Initial sample distribution

In the derivation of Eq. (1), the initial distribution of sample was assumed to be a Dirac delta function centered at the closed end of the diffusion tube. Throughout the present experiments, we have kept the injection volumes small (typically 0.1 mL to 0.2 mL of the 10 mL diffusion column volume) to mimic this assumption. In addition, we have performed simulations with different initial distributions to evaluate the effects of the initial volume and concentration profile on the measured diffusion coefficients. We have chosen to perform simulations with both square-wave and half-Gaussian sample distributions. The square-wave distribution represents a clean plug injection of sample at the head of the column, and the half-Gaussian is a convenient means to qualitatively represent extensive mixing upon injection.

The maximum of the half-Gaussian distribution was placed at the head of the diffusion column, where the mole fraction of sample to bath gas was assumed to be unity. The widths of the distributions were determined from the volume of injected sample, either 0.25 mL or 1.0 mL, of a tube of 10.0 mL total volume of length 61 cm. The simulations were carried out with diffusion coefficients (at the temperature and pressure of the simulated diffusion) of 0.1 $cm^2\ s^{-1}$ and 1.0 $cm^2\ s^{-1}$, which spans the typical range of diffusion coefficients measured in this work. The output concentration profiles were analyzed with the LTD analysis over various time ranges to find the difference between the actual and LTD-analyzed binary diffusion coefficient values (D_{12}).

All of the D_{12} derived from the LTD analysis showed slight deviations from the input coefficients that varied with the time range used in the analysis. For the 0.25 mL square wave with $D_{12} = 0.1\ cm^2\ s^{-1}$, the variation was less than 0.05% over all times typical for an LTD analysis of a diffusion coefficient of that order. The 1.0 mL square wave with $D_{12} = 0.1\ cm^2\ s^{-1}$ showed deviations up to 1.5% over typical analysis times. Similar deviations were observed with $D_{12} = 1.0\ cm^2\ s^{-1}$ for the 1.0 mL square wave, although they showed a much greater sensitivity to the time range, as expected from the curvature described above in LTD analysis plots. The 0.25 mL Gaussian distributions showed a larger error, up to 0.1% for typical analysis times with $D_{12} = 1.0\ cm^2\ s^{-1}$ and 3.0% for $D_{12} = 1.0\ cm^2\ s^{-1}$. The 1.0 mL Gaussian distributions also showed higher deviations of up to 3% for typical analysis times with $D_{12} = 1.0\ cm^2\ s^{-1}$ and varying deviations of approximately two times those of the corresponding square wave for $D_{12} = 1.0\ cm^2\ s^{-1}$ over typical analysis times.

Overall, the use of small injection volumes appears to make the shape of the distribution (derived from possible mixing in the injection) have minimal effect, although extensive mixing can affect the measured diffusion coefficient as the injection size increases. The injection of the sample perpendicular to the length of the sample tube and low injection pressure differential are anticipated to yield a clean plug injection with minimal mixing. We therefore expect the shape of the initial sample distribution to be well-represented by the square-wave distribution. Nonethelesss, to minimize the impact of the initial concentration distribution shape, we have elected to use a small (0.1 to 0.2) mL injection volume and have utilized a custom-made fitting at the head of the column that directs the injected gas at right angles to the diffusion column. Combined, these precautions are expected to make errors from the injection minimal in the present experiment.

5. Conclusion

We have constructed a reversed-chromatography apparatus for the determination of binary diffusion coefficients for a wide range of compounds at pressures from (1.5 to 7.5) bar and (200 to 723) K. Analysis of the resulting chromatograms is accomplished through a linearization derived from Laplace transform of Fick's Law to yield binary diffusion coefficients of the dilute injected sample in the bath gas. Careful measurement of temperature and pressure, systematic correction of the tube length, and consideration of nonlinear effects due to artifacts of the analytical procedure has minimized uncertainties from experimental variables. Simulations of the concentration profile in the diffusion column have demonstrated analytical procedures and experimental parameters that further minimize uncertainties due to the linearization procedure. Binary diffusion coefficients at 1.013 bar have been presented at temperatures from (300 to 723) K along with temperature dependence parameterizations for (dilute analyte–bath gas) Ar–He, He–N_2, N_2–He, and CH_4–He. The present results demonstrate the validity of the experimental and analytical procedure and pave the way for exploring the diffusion of other hydrocarbons in He, Ar, and N_2. In future work we will extend these studies to the diffusion of larger hydrocarbons, thus developing a set of data to be sound basis for theoretical models for extrapolation to higher temperatures and pressures.

Acknowledgments

We acknowledge the assistance of Nicholas Heinz for technical assistance through the construction and early validation stages of the experiment. This work was partially supported by the United States Air Force Office of Scientific Research, Julian Tishkoff, Program Manager.

Appendix A. Supplementary data

Supplementary data associated with this article can be found, in the online version, at doi:10.1016/j.chroma.2011.09.035.

References

[1] H. Wang, Chem. Phys. Lett. 325 (2000) 661.

[2] M.K. Mishra, R. Yetter, Y. Reuven, H. Rabitz, M.D. Smooke, Int. J. Chem. Kinet. 26 (1994) 437.
[3] A.T. Holley, Y. Dong, M.G. Andac, F.N. Egolfopoulos, Combust. Flame 144 (2006) 448.
[4] G. Karaiskakis, D. Gavril, J. Chromatogr. A 1037 (2004) 147.
[5] N.A. Katsanos, G. Karaiskakis, J. Chromatogr. 237 (1982) 1.
[6] G. Karaiskakis, N.A. Katsanos, A. Niotis, Chromatographia 17 (1983) 310.
[7] N.A. Katsanos, G. Karaiskakis, J. Chromatogr. 254 (1983) 15.
[8] N.A. Katsanos, G. Karaiskakis, Adv. Chromatogr. 24 (1984) 125.
[9] N.A. Katsanos, G. Karaiskakis, Analyst 112 (1987) 809.
[10] N.A. Katsanos, R. Thede, F. Roubani-Kalantzopoulou, J. Chromatogr. A 795 (1998) 133.
[11] D. Gavril, G. Karaiskakis, Instrum. Sci. Technol. 25 (1997) 217.
[12] D. Gavril, G. Karaiskakis, Chromatographia 47 (1998) 63.
[13] K.R. Atta, D. Gavril, G. Karaiskakis, Instrum. Sci. Technol. 30 (2002) 67.
[14] K.R. Atta, D. Gavril, G. Karaiskakis, J. Chromatogr. Stud. 41 (2003) 123.
[15] N.A. Katsanos, Chromatographic Science, Flow Perturbation Gas Chromatography, Vol. 42, Marcel Dekker, 1988.
[16] D. Gavril, K.R. Atta, G. Karaiskakis, Fluid Phase Equilib. 218 (2004) 177.
[17] N.A. Katsanos, D. Gavril, J. Kapolos, G. Karaiskakis, J. Colloid Interface Sci. 270 (2004) 455.
[18] N.A. Katsanos, J. Kapolos, D. Gavril, N. Bakaoukas, V. Loukopoulos, A. Koliadima, G. Karaiskakis, J. Chromatogr. A 1127 (2006) 221.
[19] D. Gavril, Catal. Today 154 (2010) 149.
[20] R.C. Reid, J.M. Prausnitz, B.E. Poling, The Properties of Gases and Liquids, 4th ed., McGraw-Hill, New York, 1987.
[21] D.R. Lide, CRC Handbook of Chemistry and Physics, 88th ed., CRC Press/Taylor and Francis, Boca Raton, FL, 2008.
[22] T.N. Bell, I.R. Shankland, P.J. Dunlop, Chem. Phys. Lett. 45 (1977) 445.
[23] P.S. Arora, P.J. Dunlop, J. Chem. Phys. 71 (1979) 2430.
[24] P.J. Dunlop, C.M. Bignell, Int. J. Thermophys. 18 (1997) 939.
[25] P.R. Bevington, D.K. Robinson, Data Reduction and Error Analysis for the Physical Sciences, 3rd ed., McGraw-Hill, Boston, 2003.
[26] E. Jones, T. Oliphant, P. Peterson, others, SciPy: Open Source Scientific Tools for Python, v. 0.6.0, http://www.scipy.org/.
[27] P.S. Arora, I.R. Shankland, T.N. Bell, M.A. Yabsley, P.J. Dunlop, Rev. Sci. Instrum. 48 (1977) 673.
[28] E.R. Marrero, E.A. Mason, J. Phys. Chem. Ref. Data 1 (1972) 3.
[29] J. Kestin, K. Knierim, E.A. Mason, B. Najafi, S.T. Ro, M. Waldman, J. Phys. Chem. Ref. Data 13 (1984) 229.
[30] W.A. Wakeham, A. Nagashima, J.V. Sengers, Experimental Thermodynamics, Vol. III. Measurement of the Transport Properties of Fluids, Blackwell Scientific, Oxford, 1991.
[31] J.C. Liner, S. Weissman, J. Chem. Phys. 56 (1972) 2288.
[32] R.D. Trengove, P.J. Dunlop, Physica A 115 (1982) 339.
[33] E.N. Fuller, J.C. Giddings, J. Gas Chromatogr. 3 (1965) 222.
[34] A.T.C. Hu, R. Kobayashi, J. Chem. Eng. Data 15 (1970) 328.
[35] F. Yang, S. Hawkes, F.T. Lindstrom, J. Am. Chem. Soc. 98 (1976) 5101.
[36] A.C. Frost, A Method for the Measurement of Binary Gas Diffusivities, Columbia University, 1967.
[37] E.N. Fuller, P.D. Schettle, J.C. Giddings, Ind. Eng. Chem. 58 (1966) 18.
[38] E.N. Fuller, K. Ensley, J.C. Giddings, J. Phys. Chem. 73 (1969) 3679.
[39] A.C. Frost, E.H. Amick, Ind. Eng. Chem. Fundam. 12 (1973) 129.
[40] P.J. Dunlop, C.M. Bignell, J. Chem. Phys. 93 (1990) 2701.
[41] W.H. Press, S.A. Teukolsky, W.T. Vetterling, B.P. Flannery, Numerical Recipes in C: The Art of Scientific Computing, 2nd ed., Cambridge University Press, Cambridge, 2002.
[42] E. Anderson, Z. Bai, C. Bischof, S. Blackford, J. Demmel, J. Dongarra, J.D. Croz, A. Greenbaum, S. Hammarling, A. McKenney, D. Sorensen, LAPACK Users' Guide, 3rd ed., Society for Industrial and Applied Mathematics, Philadelphia, 1999.